Interface sharpening in CoFeB magnetic tunnel junctions

A. T. G. Pym, A. Lamperti, and B. K. Tanner[a)]
Department of Physics, University of Durham, South Road, Durham, DH1 3LE, United Kingdom

T. Dimopoulos, M. Rührig, and J. Wecker
Siemens AG, Corporate Technology MM1, 91502 Erlangen, Germany

(Received 21 December 2005; accepted 20 March 2006; published online 20 April 2006)

We report grazing incidence x-ray scattering evidence for sharpening of the interface between amorphous $Co_{60}Fe_{20}B_{20}$ and AlO_x during *in situ* annealing below the $Co_{60}Fe_{20}B_{20}$ crystallization temperature. Enhancement of the interference fringe amplitude in the specular scatter and the absence of changes in the diffuse scatter indicate that the sharpening is not a reduction in topological roughness but a reduction in the width of the chemical composition profile across the interface. The temperature at which the sharpening occurs corresponds to that at which a maximum is found in the tunneling magnetoresistance of magnetic tunnel junctions. © *2006 American Institute of Physics*. [DOI: 10.1063/1.2195774]

Various uses have been proposed for magnetic tunnel junctions (MTJs) following the discovery of large tunnel-magnetoresistance (TMR) at room temperature.[1] While TMR values of 230% were recently observed in MgO based MTJs, the resistance area product (RA) was very high, at 420 $\Omega\ \mu m^2$, and significant work is needed before these systems can be incorporated into practical devices.[2] Most work has been focused on tunnel barriers of AlO_x where TMRs up to ~70% have been observed[3] with very low RA products of $<1\ \Omega\ \mu m^2$. The high TMR exhibited by such AlO_x MTJs is partially attributed to the excellent quality of the interfaces. Systematic differences between barrier widths determined by x-ray scattering and electrical measurements[4] in devices with a lower TMR have been attributed to the effects of nonconformal roughness, whereby the tunneling begins locally at positions of minimum thickness.

Amorphous CoFeB electrodes have the advantage of being homogenous in the very small scales required for high-density recording media which are not possible with polycrystalline electrodes. Associated with crystallization at elevated temperature is a rise in coercivity[5] of AlO_x MTJs fabricated with $Co_{60}Fe_{20}B_{20}$ electrodes.[6] There is also a similar rise in the RA product. However, prior to crystallization, there is a significant increase in TMR (Ref. 7) and a low-temperature anneal can significantly enhance the performance of MTJs. Recent high-resolution electron microscopy results have been interpreted as evidence for an association between the smoothness or sharpness of the electrode/barrier interface and a high TMR,[8,9] and the micrographs of Li *et al.*[10] suggest incipient crystallization of the CoFeB on annealing at 265 °C. We have undertaken *in situ* x-ray reflectivity measurements to search for changes in the interface structure during annealing below the crystallization temperature and relate the improved magnetotransport to such structural changes.

High-resolution grazing incidence x-ray scattering experiments have been performed at the SRS synchrotron radiation source at Daresbury Laboratory. *In situ* reflectivity measurements were made during annealing *in vacuo* in the induction furnace on station 2.3 using alignment and data collection techniques that are now standard. A wavelength λ of 0.13 nm was chosen to maximize the intensity from the bending magnet; a channel-cut 111 Si crystal acted as the monochromator. Samples were prepared by magnetron sputtering on plasma-etched thermally oxidized Si wafers. An exchange bias pinned $Co_{60}Fe_{20}B_{20}$ electrode and AlO_x tunnel barrier were deposited on a SiO_2 substrate with an IrMn antiferromagnetic pinning layer: SiO_2/Ta(5 nm)/Ru(30 nm)/IrMn(8 nm)/$Co_{60}Fe_{20}B_{20}$(3 nm)/AlO_x(1.2 nm)/Ta(5 nm)/Ru(5 nm). No free electrode was deposited on the AlO_x in order for there to be only one CoFeB/AlO_x interface. The reflectivity was measured continuously during annealing.

Off-specular measurements indicated that the interfaces were all very smooth, resulting in very little diffuse scatter. The specular scatter profile was very rich in detail (Fig. 1) and true specular scatter extended out to a detector angle Φ of about 6° (or $q_z=(2\pi/\lambda)\sin\Phi=5.05\ nm^{-1}$). (The true specular scatter is the measured specular intensity minus the

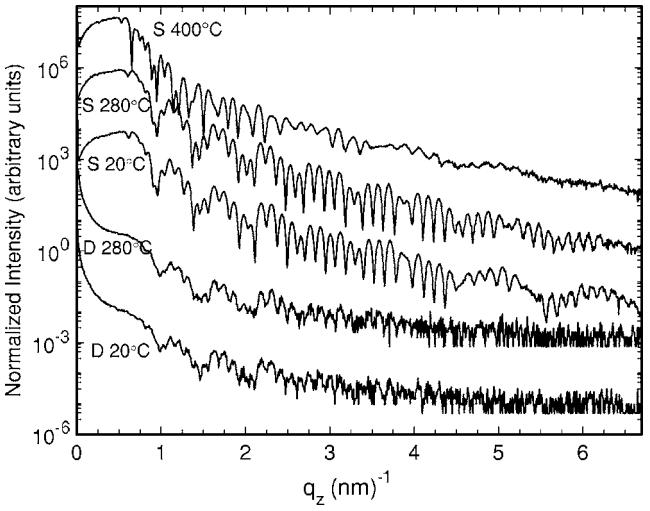

FIG. 1. True specular scatter (upper three curves denoted as S) for a sample prior to anneal (20 °C) and after heating to temperatures of 280 °C and 400 °C. The two lower curves are the longitudinal diffuse scatter (denoted as D) at 20 and 280 °C. Here, the sample is offset −0.1° from the specular position, the detector and sample being scanned in the ratio of 2:1 as in a specular scan. (The D20 °C curve is scaled, and hence displaced, by a factor of 0.01, the S280 °C by 100 and the S400 °C by 10,000 for clarity.)

[a)]Electronic mail: b.k.tanner@durham.ac.uk

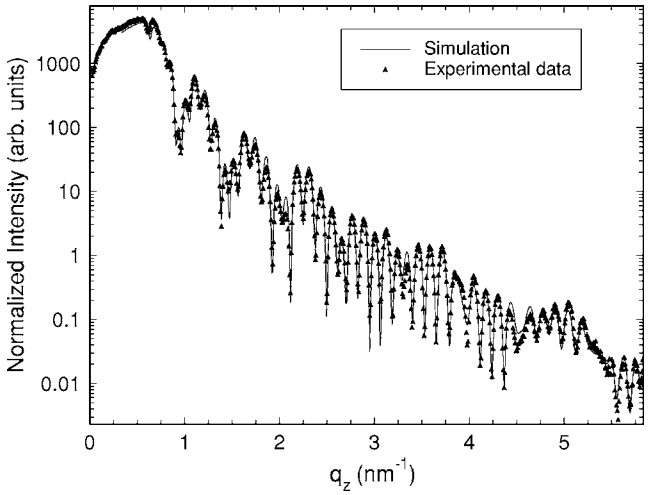

FIG. 2. Experimental and simulated specular reflectivity profile at 20 °C.

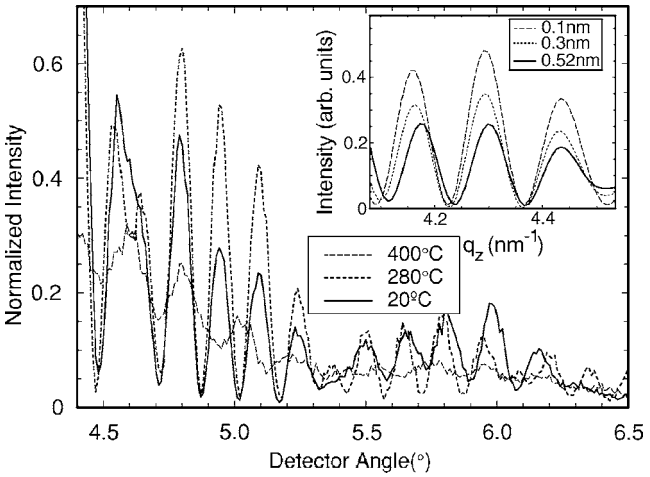

FIG. 3. Fringe amplitude (on a linear scale) in the reflectivity profile, intensity vs q_z plot, for various annealing temperatures. (Inset shows fringe amplitude as a function of interface width.)

forward diffuse scatter measured in an off-specular coupled specimen-detector scan with the sample offset about 0.1° from the specular condition.) There was little change in many of the interference fringes between samples as grown and after annealing to 280 °C. In particular, the low-frequency modulation, of about 0.6° in detector angle ($\Delta q_z = 0.5$ nm^{-1}), which is associated with the surface oxide layer, was not affected by the annealing, indicating that no significant degradation of the top surface was occurring. There is a very great change in the reflectivity curve between 340 °C and 400 °C, corresponding to the crystallization of the $Co_{60}Fe_{20}B_{20}$. In particular, by 400 °C, there is a significant reduction in the fringe amplitude, characteristic of increased interface width.

The specular scatter of the as-grown samples was modeled using the Bede REFS-MERCURY software which uses a genetic algorithm to refine the model structure to the experimental data. An example of the level of correspondence achieved is shown in Fig 2. The best fit parameters are listed in Table I.

There are regions of the reflectivity profile where a systematic change in the fringe structure is observed as a function of annealing temperature, a particularly prominent one being in the range of a scattering vector between 4 and 5.5 nm^{-1} (see Fig. 1). Here, as the annealing temperature is raised, the fringe amplitude increases markedly. Upon raising the temperature, the reflectivity changes occurred rapidly and we were unable to record the time dependence. By the typical time of 10 min, taken for the temperature ramp to take place, equilibrium had been reached. The data shown in Fig. 3 correspond to the stable fringe amplitude, in this case after annealing for 2 h.

TABLE I. Best fit parameters for the 20 °C specular reflectivity.

Layer	Material	Thickness (nm)	Width of top interface (nm)	Density (%)
1	RuO_2	0.67±0.01	0.13±0.03	18±12
2	Ru	5.52±0.04	0.40±0.02	99±1
3	Ta	4.21±0.03	0.10±0.07	95±1
4	AlO_x	2.14±0.03	0.44±0.06	53±5
5	$Co_{60}Fe_{20}B_{20}$	1.73±0.06	0.52±0.03	100±1
6	IrMn	6.69±0.06	0.70±0.07	100±1
7	Ru	27.58±0.02	0.27±0.02	95±1
8	Ta	4.49±0.01	0.10±0.03	101±1
Substrate	SiO_2	···	0.23±0.01	101±7

The key amplitude changes occur at quite high scattering vector, corresponding to changes to small out-of-plane length scales. In addition, there is an additional fringe appearing between 5 and 7 nm^{-1} and corresponding shift in the fringe maxima. Four independent annealing runs have been carried out, all exhibiting the same fringe amplitude increase and fringe shift.

Extensive modeling work on specular x-ray reflectivity data has shown that an increase in width of a buried interface, whether as a result of topological roughness or chemical intermixing, always results in reduction of interference fringe amplitude.[11] The increase in interference fringe amplitude shown in Fig. 3 can only be explained by a reduction in the width of one or more interfaces during the annealing process.

It has proved to be difficult to model the change in the interface width by fitting the whole reflectivity profile and allowing all parameters to float freely. We have therefore fitted the data at 20 °C very carefully, deducing a $Co_{60}Fe_{20}B_{20}/AlO_x$ interface width of 0.52±0.03 nm, and then simulated the effect of changing this interface width in the region wavevector in which the changes in fringe amplitude were observed experimentally. This simulation is shown as an inset to Fig 3. Using the 20 °C point as a standard, comparison between the observed fringe amplitude change and the simulation enables us to deduce the $Co_{60}Fe_{20}B_{20}/AlO_x$ interface width as a function of annealing temperature (Fig. 4).

If the interface width reduction was due to a topological smoothing of the interface, a corresponding reduction in the diffuse scatter should have been observed. In both transverse and longitudinal scans (Fig. 1) of the diffuse scatter in reciprocal space, we observed no such change. There is remarkably little diffuse scatter from this system, as a result of the interfaces being extremely smooth, and we were unable to measure the diffuse scatter at the wavevector corresponding to that at which the specular scatter was found to change. We therefore performed similar experiments on $[Co_{60}Fe_{20}B_{20}/AlO_x]_5$ multilayers. An increase in the amplitude of the specular Bragg peak was observed upon anneal-

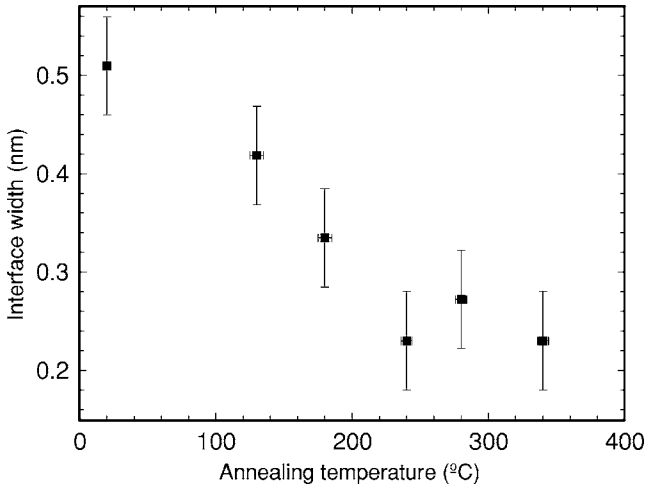

FIG. 4. Equilibrium root-mean-square amplitude of the width of the $CoFeB/AlO_x$ interface as a function of annealing temperature.

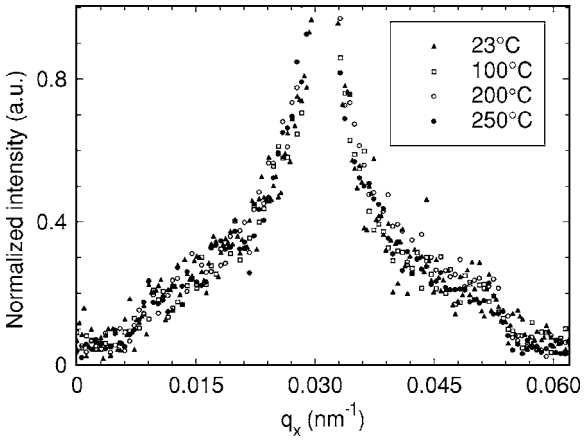

FIG. 5. Transverse scans through the first Bragg peak from a $[CoFeB/AlO_x]_5$ multilayer at several annealing temperatures.

ing to 280 °C. Unlike the data in Fig. 1, the result must be viewed with caution as there is no built-in verification that the alignment had not altered, thereby resulting in an artificial change in the specular intensity. However, measurements of the diffuse scatter through the first multilayer Bragg peak in the q_x direction of reciprocal space (Fig. 5) are not subject to this artefact. At all temperatures studied, there is no change in the amount or distribution of the diffuse scatter. Further, there was no change in the height or width of the associated Bragg peak in the diffuse scatter recorded in a coupled scan with the specimen offset from the specular condition. This is firm confirmation that the conformal topological roughness does not change during the annealing. The overall conclusion is that the $Co_{60}Fe_{20}B_{20}/AlO_x$ interface width reduction arises from a sharpening of the composition change across the interface, diffusion driven by the chemical potential. As the TMR rises to a maximum at the temperature at which the interface width falls to its lowest value, the implication is that the tunneling probability is enhanced by the sharpening of the interface.

The temperature at which the x-ray scattering indicates sharpening of the $Co_{60}Fe_{20}B_{20}/AlO_x$ interface corresponds directly to the temperature at which the maximum TMR occurs.[7] This sharpening takes place in the amorphous phase of $Co_{60}Fe_{20}B_{20}$, well below the crystallization temperature determined by high-angle x-ray diffraction, and provides direct evidence of the importance of interface structure in determining the magnitude of the TMR in MTJ devices.

Financial support was partly provided by the UK Engineering and Physical Sciences Research Council. One of the authors (A.L.) acknowledges the financial support provided through the European Community's Marie Curie actions (Research Training Networks) under Contract No. MRTN-CT-2003-504462, ULTRASMOOTH. Thanks are expressed to Dr. Tony Bell and the staff of Daresbury Laboratory for technical support.

[1] J. S. Moodera, L. R. Kinder, T. M. Wong, and R. Meservey, Phys. Rev. Lett. **74**, 3273 (1995).
[2] D. D. Djayaprawira, K. Tsunekawa, M. Nagai, H. Maehara, S. Yamagata, N. Watanabe, S. Yuasa, Y. Suzuki, and K. Ando, Appl. Phys. Lett. **86**, 092502 (2005).
[3] D. X. Wang, C. Nordman, J. M. Daughton, Z. H. Qian, and J. Fink, IEEE Trans. Magn. **40**, 2269 (2004).
[4] J. D. R. Buchanan, T. P. Hase, B. K. Tanner, N. D. Hughes, and R. J. Hicken, Appl. Phys. Lett. **81**, 751 (2002).
[5] N. Wiese, T. Dimopoulos, M. Rührig, J. Wecker, H. Brückl, and G. Reiss, J. Magn. Magn. Mater. **290**, 1427 (2005).
[6] S. Cardoso, C. Cacaco, R. Ferreira, L. Peiera, M. Rickart, P. P. Freitas, N. Franco, J. Gouveia, and N. P. Barradas, J. Appl. Phys. **97**, 10C916 (2005).
[7] T. Dimopoulos, G. Gieres, J. Wecker, N. Weise, and M. D. Sacher, J. Appl. Phys. **96**, 6382 (2004).
[8] J. Y. Bae, W. C. Lim, H. J. Kim, T. W. Kim, and T. D. Lee, Jpn. J. Appl. Phys., Part 1 **44**, 3002 (2005).
[9] J. Y. Bae, W. C. Lim, H. J. Kim, T. W. Kim, and T. D. Lee, IEEE Trans. Magn. **41**, 2676 (2005).
[10] F. F. Li, R. Sharif, L. X. Jiang, X. Q. Zhang, X. F. Han, Y. Wang, and Z. Zhang, J. Appl. Phys. **98**, 113710 (2005).
[11] V. Holy, U. Pietsch, and T. Baumbach, *High Resolution X-ray Scattering from Thin Films to Lateral Nanostructures*, Springer Tracts in Modern Physics Vol. 149, 2nd ed. (Springer, Berlin, 2004).